We are IntechOpen, the world's leading publisher of Open Access books Built by scientists, for scientists

4,800
Open access books available

122,000
International authors and editors

135M
Downloads

Our authors are among the

154
Countries delivered to

TOP 1%
most cited scientists

12.2%
Contributors from top 500 universities

CLARIVATE ANALYTICS BOOK CITATION INDEX INDEXED

WEB OF SCIENCE™

Selection of our books indexed in the Book Citation Index in Web of Science™ Core Collection (BKCI)

Interested in publishing with us?
Contact book.department@intechopen.com

Numbers displayed above are based on latest data collected.
For more information visit www.intechopen.com

2

Locomotion of an Underactuated Biped Robot Using a Tail

Fernando Juan Berenguer and Félix Monasterio-Huelin
Universidad Europea de Madrid, Universidad Politécnica de Madrid
Spain

1. Introduction

At the present there exist a high number of commercial biped robots, generally humanoids, used within the area of service robotics, mainly in the field of exhibition and entertainment (Ambrose et al., 2006; Wahde & Pettersson, 2002). One of the main problems of these robots is their high power and energy consumption, which limits mainly their autonomy. It could be attributed to, for example, the high number of actuated joints (about 20), and also because the study of energy consumption is not often considered during the planning of movements. In addition, these systems require high precision in their motions and high frequency response.

In order to solve these important problems there exist various solutions not used yet commercially, which are mainly based on the use of passive joints, thus reducing the number of actuated joints (Alexander, 2005; Collins et al., 2005; Kuo, 1999). The consumption of these systems is better optimized, although their control and planning require more complex schemes for the accomplishment of certain complex trajectories.

The main aim of our research is the design of biped robots with passive joints that require low energy consumption. In particular our work is centred on the one hand, in studying the advantages and disadvantages of considering a tail as the main element that generates the motion, and on the other hand, in trying to reduce the energy consumption in two ways, by means of generating a smooth contact between the feet and the ground, with minimum loss of energy, and by using a spring mechanism to reduce the mechanical energy needed to obtain the oscillating motion of the tail. In addition, our present work focuses on the study of a biped mechanism of a simple design and construction, able to walk using only a single actuated joint. This is a low cost system, and its easy design and construction make it interesting for commercial and educational applications.

2. About passive bipeds and bipeds with a tail

The interaction between morphology and control is in the centre of the more recent research and debates in robotics. The main question is how to design a robot that exhibit a repertoire of behaviours.

In the field of walking robots there are two main extreme approaches. Oldest focused on the intrinsic properties of the robot, leaving into the hands of control the task of achieving the desired movements. The more recent takes into account as a guiding principle, the

Source: Bioinspiration and Robotics: Walking and Climbing Robots, Book edited by: Maki K. Habib
ISBN 978-3-902613-15-8, pp. 544, I-Tech, Vienna, Austria, EU, September 2007

interaction with the environment in a cooperative manner. Both approaches have at the present, open and unresolved questions and problems.

The main characteristic of (biped) walkers is the abrupt kinematic change between the aerial phase and the support phase. The main problem is how to achieve a rhythmical walk.

Control centred approaches must generate exact trajectories to guide the robot from one to the next support, taking into account the stability region of the aerial phase. Normally the considered region is a pressure region which has a fictitious point (the Zero Moment Point, ZMP (Vukobratovic, 1969)) on the ground plane where the torques around the axes that define this plane are equal to zero. Expanding the ZMP concept to running biped robots is the natural continuation of this approach (Kajita et al., 2007).

The discovery of self-stabilizing dynamic properties of passive mechanisms by McGeer (McGeer, 1990), opens the doors to the environmental (or dynamic) approach: a simple mechanism which can walk down a slope without control nor actuation. He takes into account the terrestrial gravity as the only interaction with the world, imposing two main principles: the conservation of mechanical energy and the conservation of angular momentum in the contact instant of the leg with the ground. From the second we obtain a constraint equation that, added to the dynamical equation, gives strict initial conditions for joint positions and joint velocities to achieve a stable walk. The result is a periodic gait: a limit cycle. Numerous biped robots have been developed following this property (Collins et al., 2005), showing the noteworthy energetic efficiency in contrast to the ZMP approach (Gomes & Ruina, 2005).

This approach is related with those that make an explicit use of the behaviour emergence from the interaction of body and environment, that is, those that consider the self-organizing properties of the nature. Behaviour-based robotic is an important engineering example (Pfeifer & Scheier, 1999) to understand sensory-motor coordination, or in general the perception-action relation. How to exploit the above-mentioned passive properties of biped robots with the incorporation of sensors is studied in (Iida & Pfeifer, 2006).

In order to close this brief review, we need to mention biped robots with a tail. Almost none of the robots of this type make of the tail a functional element, but there are some exceptions. For example in (Takita et al., 2003) the tail and the neck are designed with the objective of stabilizing the robot walks.

3. Mechanism model and gait description

In this section the proposed model of the biped mechanism and the way it performs a gait are presented. We show the evolution of the kinematic model indicating its components and parameters, and we explain how this system is able to walk using only one actuator that moves a tail in an oscillating way.

3.1 Mechanism model

The walking mechanism consists of a light body, a tail connected to it, and two legs. Each leg is formed by a parallel link mechanism and a flat rectangular foot. The tail, with an almost horizontal displacement, works as a counterbalance and controls the movement of the biped. The kinematic model of the system is shown in Fig. 1 and it is a 3D biped model. This figure displays the masses of each independent link, and the main lengths involved in the design. We don't consider in this work the link inertial moments for reducing the expression's complexity and required parameters definition.

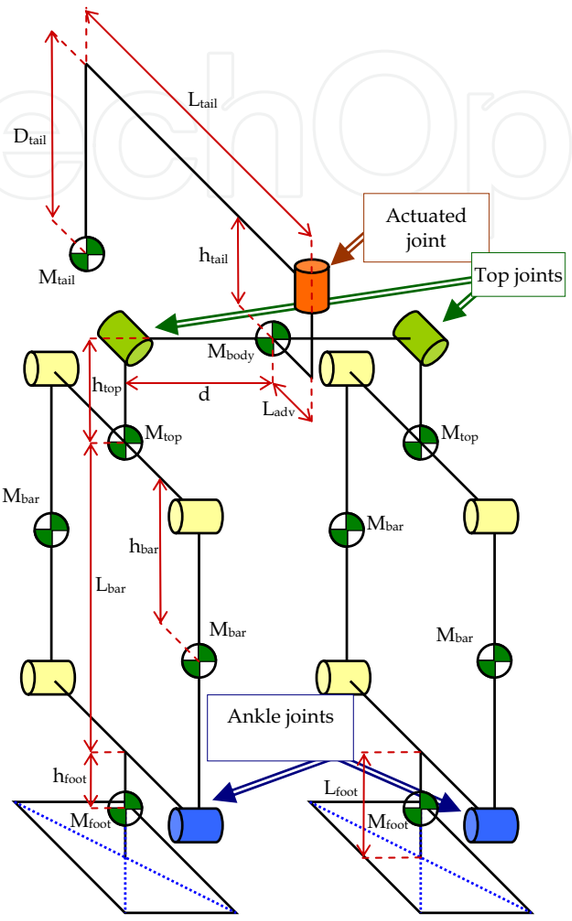

Figure 1. Model of the biped mechanism

The mechanism has 11 joints. The joint connecting the tail to the body is actuated by an electric motor and it is the only actuated degree of freedom. Connecting the body to each leg are the top joints. Their rotation axis is normal to the frontal plane, so they allow the mechanism to raise a foot while both feet remain parallel to the ground. We define de parameter B_{top} as the friction coefficient at these joints. Finally, each parallel link mechanism has four joints, and we consider that in one of these joints (the ankle joint) there is a spring with friction. Both ankles systems have the same parameters values K_{ank}, B_{ank} and θ_{0ank}, which represent the stiffness, friction and equilibrium position in each ankle joint. Due to the characteristics of the parallel link mechanism, these four joints represent only one passive degree of freedom for each leg of the mechanism.

In summary, the model has four passive degrees of freedom and one actuated degree of freedom.

3.2 Gait description

The tail of the robot moves in an almost horizontal plane. When tail is in a lateral position of the mechanism, its mass acts as a counterbalance and produces the rise of one of the feet. Then a step begins. We will define and describe here seven phases during a stride. Fig. 2 shows these phases starting at an equilibrium position of the system with the tail in its central position.

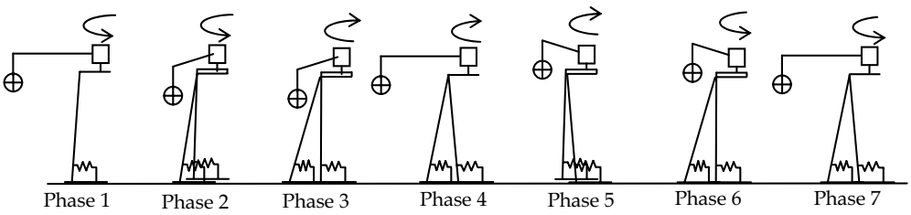

Figure 2. Phases during a stride

Phase 1: Displacement of the tail to a lateral of the mechanism: Both springs hold the weight of the mechanism, and this one stays almost vertical. We use linear springs in Fig. 2 for a better understanding of their effect and because they have been used in the construction of our first real prototype Zappa that we will present in section 8.

Phase 2: Rise of one foot and single support phase. When a foot rises, only one spring holds the body, so the stance leg falls forward to a new equilibrium position. In this phase, kinetic and potential energies are transformed into elastic energy and stored in the ankle springs. The swing leg moves forward as a pendulum.

Phase 3: Contact of the swing leg with the ground. At this moment the greater kinetic energy losses are due to the collision. We must calibrate the mechanism trying to reduce the velocities at this moment and provide a smooth contact between the foot and the ground.

Phase 4: Movement of the tail to the other side. In this double support phase, the projection of the centre of masses of the mechanism moves from one foot to the other. The body moves backwards to a position in which both springs generate opposing torques.

Phase 5: Rise of the second foot. In this phase, the spring of the foot that is in the ground produces enough torque to take the body forward again.

Phase 6: New contact of a swing leg with the ground. Same as phase 3.

Phase 7: New displacement of the tail during a double support phase. If a new stride is desired, this phase represents returning to phase 1. If the tail stops in the middle position, the system will stay in a steady configuration with no energy cost.

The mechanism is able to walk forward, and if the tail is passed to the frontal side, then it also walks backwards. In (Berenguer&Monasterio, 2006), we show how this biped can also turn by means of small amplitude periodic motions of the tail and by sliding it's feet, but this motion results in a few elegant turning method. Turn can be achieved by adding a new joint in each leg and performing stable rise of the feet. We will see in the next section that this model has this last capability.

4. Necessary conditions for generating the gait

At low stride frequencies, basically the mechanism walks if it is able to rise its feet, move forward its body, and maintain its centre of gravity (CoG) into the support area. So, in this section we analyze the necessary conditions to reach these three characteristics. These conditions allow designing the tail in order to obtain a stable rise of the feet, and on the other hand, they establish the procedure for selecting the ankle parameters of the system to obtain the advance of the robot. The displacement of the system's CoG will be also introduced in this section because it determines the necessary support area during walking and therefore the required minimum size of the feet. We will consider static and quasi-static cases, we mean, we will not consider the velocities effects or overshoots in oscillating motions, so the conclusions are valid at low velocities and for over-damped spring systems.

4.1 Design of the tail for a stable rise of the foot

The weight of the tail and its length must be such that the body and a leg could rise under a certain condition. When a leg rises, it is desirable that it reaches a steady state so that the control of the mechanism is simpler. The passive top joints will allow rising of a foot with no need to incline laterally the stance leg. Fig. 3 shows two situations from a frontal view of the mechanism. In (a), the foot does not rise, and in (b), the foot is raised. The parameter M_{leg} is the total mass of one leg. The D_{tail} parameter represents a downwards displacement of the centre of masses of the tail and the h_{tail} parameter stays upwards in the model for its identification in a real system, because it allows the tail motion without collision with the legs.

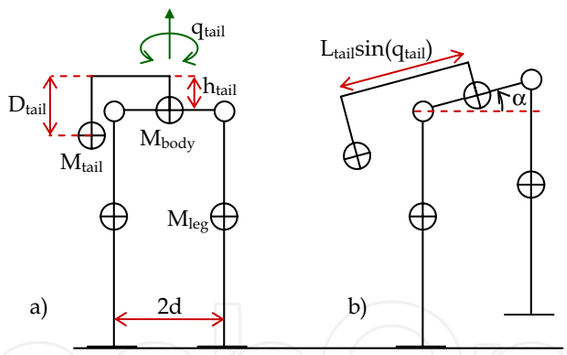

Figure 3. a) Double support configuration, b) Configuration with a raised foot

To produce the rise of the foot, the moment of the gravitational force on the tail mass must be greater than the moments of the gravitational forces on both the body mass and the mass of one leg. This condition leads to the following expression:

$$M_{tail}\left(\left|\sin(q_{tail})\right|L_{tail}-d\right)>d\left(M_{body}+2M_{leg}\right) \tag{1}$$

Here q_{tail} is the position of the tail joint, and its value is 0 radians when the tail is centred and $\pm\pi/2$ radians when it is in a maximum lateral position. From (1), if the mass of the tail (M_{tail}) is known, the minimum length of the tail required to raise the foot is given by:

$$L_{tail} = d\left(1 + \frac{M_{body} + 2M_{leg}}{M_{tail}}\right) \tag{2}$$

When condition (1) is satisfied, if the body has an inclination angle α, and the joint of the tail is in a fixed position (q_{tail}), the moments at the top joint due to the tail and the body&leg set are respectively:

$$\begin{aligned} Mt_{tail} &= M_{tail} g\left((h_{tail} - D_{tail})\sin(\alpha) + (|\sin(q_{tail})|L_{tail} - d)\cos(\alpha)\right) \\ Mt_{body\&leg} &= \left(M_{body} + 2M_{leg}\right) gd\cos(\alpha) \end{aligned} \tag{3}$$

Using (1), we deduce that if $h_{tail}>D_{tail}$, then $Mt_{tail}>Mt_{body\&leg}$ for any inclination α, and therefore the system is in an unstable configuration. We analysed this case in (Berenguer&Monasterio, 2006), and it was necessary to use an adjustable friction coefficient B_{top} in the top joints for controlling the biped movements.

If $h_{tail}<D_{tail}$, then there exists an inclination α_0, so that $Mt_{tail}=Mt_{body\&leg}$, and if there is friction in the top joints, α_0 represents a stable equilibrium inclination angle of the body.

From (3) the D_{tail} value needed for a desired α_0, when the tail is fixed in a position q_{tail}, is given by:

$$D_{tail} = h_{tail} - \frac{\left(M_{body} + 2M_{leg} + M_{tail}\right)d - M_{tail}|\sin(q_{tail})|L_{tail}}{M_{tail} tg(\alpha_0)} \tag{4}$$

Some of the important advantages that using a stable inclination angle provides are the following ones:

- We can consider the top joints as passive joints with negligible friction. In the theoretical model and simulations, a parameter in the design disappears, since now we consider the friction in the top joints negligible ($B_{top}\approx 0$).
- The inclination of the body depends now on the position of the tail and goes through successive stable states.
- The length of a single support phase is not limited in time. It allows the system to remain with a foot raised during an indefinite time.
- The yaw turn of the mechanism can be reached during a single support phase by adding new joints in the feet or the hip of the mechanism.
- It is possible to vary the speed of advance in a stable form by changing the oscillation frequency of the tail, with no need to consider the length of the single support phase.

4.2 Design of the springs and friction at the ankle joints

If the ankles equilibrium position (θ_{0ank}) is zero and stable, then, when the mechanism rise a foot due to slow tail oscillation, the body and the legs don't move in the forward direction and the mechanism doesn't advance. It is necessary that the ankle equilibrium position will be different from zero in this case. Afterwards, in section 5, we will see that at higher tail oscillation frequencies, the tail produces a force in the X direction over the body that generates the body oscillation and allows the system to walk even with θ_{0ank} equals to zero.

We present now a theoretical approach for the selection of the parameters that define the springs and friction at the ankle joints of the mechanism. For this purpose we analyze the configuration of the system at the moment of contact between the foot in the air and the

ground, that is, phases 3 and 6 shown in Figure 2. If this configuration is an equilibrium state for both legs, and is reached without overshoot at the moment at which the inclination velocity of the body is null, then the kinetic energy losses in the collision will be minimum.
In order to obtain simple expressions for the design, we consider the system decoupled into two parts: The swing leg as a pendulum with parallel links (Figure 4.a), and the stance leg as a parallel link system fixed to the ground (Figure 4.b).

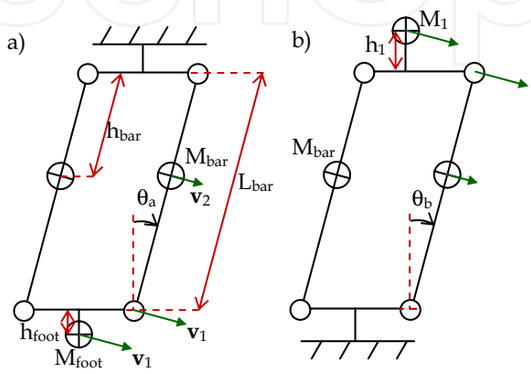

Figure 4. (a) Pendulum model, (b) parallel link system model

The angles θ_a and θ_b in Figure 4 are the generalized coordinates that represent the degree of freedom of each system. We suppose that the joint where the angle is showed in both systems, is the ankle joint of each leg, and a spring with friction exists which generates a torque τ following a classic linear model, given by expression (5). In this expression θ is the position of the joint, θ_{0ank} is the equilibrium position of the spring, K_{ank} is the spring constant, and B_{ank} is the friction coefficient.

$$\tau = -K_{ank}(\theta - \theta_{0ank}) - B_{ank}\dot{\theta} \tag{5}$$

The equations of motion that we obtain for these two systems, and the values that we assign to angles θ_a and θ_b, based on the desired step length, will allow us to select the spring parameters.
We use the Euler-Lagrange method to derive the equations of motion. For the system in Figure 4.a, Kinetic energy T_a and potential energy V_a (with respect to the position of the foot when θ_a=0rad) are given by:

$$T_a = \frac{1}{2}M_{foot}v_1^2 + M_{bar}v_2^2 + J_{bar,a}\dot{\theta}_a^2 = \frac{1}{2}J_a\dot{\theta}_a^2 \tag{6}$$

$$\begin{aligned} V_a &= M_{foot}g(1-\cos(\theta_a))L_{bar} + 2M_{bar}g(h_{foot} + L_{bar} - \cos(\theta_a)h_{bar}) = \\ &= C_a - G_a\cos(\theta_a) \end{aligned} \tag{7}$$

In (6), v_1 and v_2 are the magnitude of vectors $\mathbf{v}_1$ and $\mathbf{v}_2$ shown in the Figure 4.a. $J_{bar,a}$ is the moment of inertia of each vertical parallel bar, with respect to the rotation axis of a lower joint. We have defined for greater clarity the constants J_a, G_a and C_a, and their values are:

$$\begin{aligned} J_a &= M_{foot}L_{bar}^2 + 2M_{bar}h_{bar}^2 + 2J_{bar,a} \\ G_a &= M_{foot}gL_{bar} + 2M_{bar}gh_{bar} \\ C_a &= M_{foot}gL_{bar} + 2M_{bar}g(h_{foot} + L_{bar}) \end{aligned} \tag{8}$$

In the same way, the energies for the system in Figure 4.b are:

$$T_b = \frac{1}{2}M_1L_{bar}^2\dot{\theta}_b^2 + M_{bar}(L_{bar} - h_{bar})^2\dot{\theta}_b^2 + J_{bar,b}\dot{\theta}_b^2 = \frac{1}{2}J_b\dot{\theta}_b^2 \tag{9}$$

$$\begin{aligned} V_b &= M_1g(h_1 + L_{bar}\cos(\theta_b)) + 2M_{bar}g(L_{bar} - h_{bar})\cos(\theta_b) = \\ &= C_b + G_b\cos(\theta_b) \end{aligned} \tag{10}$$

Where,

$$\begin{aligned} M_1 &= M_{tail} + M_{body} + M_{top} + M_{leg} \\ J_b &= M_1L_{bar}^2 + 2M_{bar}(L_{bar} - h_{bar})^2 + 2J_{bar,b} \\ G_b &= M_1gL_{bar} + 2M_{bar}g(L_{bar} - h_{bar}) \\ C_b &= M_1gh_1 \end{aligned} \tag{11}$$

The parameter h_1 is the height of the mass M_1 relative to the upper joints, and since it does not affect the behaviour of the system, we do not calculate its value here. Now, $J_{bar,b}$ is the moment of inertia of each parallel bar, with respect to the rotation axis of an upper joint.
Applying the Euler-Lagrange equation to the lagrangian (L = T - V) in each case, and using (5), we obtain the equations of motion for these systems:

$$J_a\ddot{\theta}_a + G_a\sin(\theta_a) = -K_{ank}(\theta_a - \theta_{0ank}) - B_{ank}\dot{\theta}_a \tag{12}$$

$$J_b\ddot{\theta}_b - G_b\sin(\theta_b) = -K_{ank}(\theta_b - \theta_{0ank}) - B_{ank}\dot{\theta}_b \tag{13}$$

If both systems are in an equilibrium configuration, the two following equations will be fulfilled together:

$$K_{ank}(\theta_a - \theta_{0ank}) + G_a\sin(\theta_a) = 0 \tag{14}$$

$$K_{ank}(\theta_b - \theta_{0ank}) - G_b\sin(\theta_b) = 0 \tag{15}$$

Once fixed the values of θ_a and θ_b, we calculate the values of K_{ank} and θ_{0ank} for the springs with the next equations:

$$K_{ank} = \frac{G_a\sin(\theta_a) + G_b\sin(\theta_b)}{\theta_b - \theta_a} \tag{16}$$

$$\theta_{0ank} = \theta_b - \frac{G_b}{K_{ank}}\sin(\theta_b) \tag{17}$$

For obtaining a θ_{0ank} value different from zero, θ_a must be a small negative angle different from zero, -0.01rad for example. Once selected θ_a, the relation between the step length (L_{step}) and the necessary angle θ_b is given by:

$$\theta_b = -\arcsin\left(\frac{L_{step}}{L_{bar}} - \sin(\theta_a)\right) \tag{18}$$

Finally, if we linearize equation (13), and compare the result with a second order system equation, we find that the necessary value of B_{ank} to obtain critical damping is:

$$B_{ank} = 2\sqrt{(K_{ank} - G_b)J_b} \tag{19}$$

When the contact takes place, the top joints of the legs will be at different height and the body will have an inclination α (defined in Figure 3.b). The minimum inclination module $|\alpha_{min}|$ that the body must reach for obtaining a desired configuration at contact instant is given by Equation (20).

$$|\alpha_{min}| = \arcsin\left(\frac{L_{bar}(\cos(\theta_a) - \cos(\theta_b))}{2d}\right) \tag{20}$$

4.3 Approximation of the Center of Gravity projection trajectory

In this quasi-static study, we can obtain an estimation of the necessary support area during walking, and the minimum required feet size, by means of approximating the Centre of Gravity (CoG) projection trajectory instead of the Zero Moment Point (ZMP) trajectory.

For this approximation we will assume that the tail moves side to side only when the body is in a central position between both feet, during a double support phase (Phase 4 in figure 2), and the tail stands in a lateral position ($q_{tail}=\pm\pi/2$) the rest of time, during the double and single support phases (Phases 5 and 6 in figure 2). For additional simplicity, we assume that legs and feet are massless, and the body center of masses is located at the tail-joint axis.

In the first case, because only the tail mass moves, the CoG describes a circumference arc with radius R_1 given by:

$$R_1 = \frac{M_{tail}}{M_{total}} L_{tail} \tag{21}$$

Next, when the central body moves forward and backward, the CoG describes a straight line parallel to the body trajectory, with maximum length equal to the body crossed distance. This length is approximately 3/2 of the step length (L_{step}) and depends on the body, legs and feet masses. Then, during a stride starting with the tail in its central position and both feet on the ground, an approximation of the CoG trajectory is shown in figure 5.

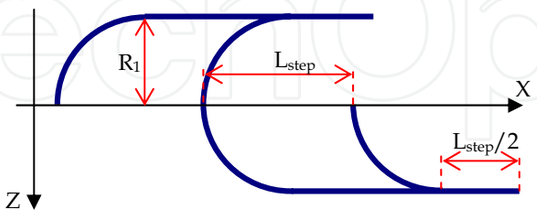

Figure 5. Approximation of the CoG trajectory during a stride

The required length of the feet in the X direction is given by $R_1+3/2L_{step}$ and the distance between the outside of the feet must be at least $2R_1$. We can establish that this biped mechanism needs a relatively large support area and feet length that depends mainly on the tail length and mass, and on the desired step length.

5. Study of the system behaviour with oscillation frequency variation

This section focuses on studying the effect of increasing the oscillation frequency that allows the mechanism to increase its speed. We will see how the conditions of the previous section are modified by means of analyzing a simpler system, a horizontal pendulum with rotational actuated joint.

5.1 ZMP trajectory and generated forces at the tail joint axis

We can obtain important information about the effect of the tail over the mechanism behaviour when the oscillating frequency increases, by studying the system shown in figure 6. This is a two-links mechanism with only one joint (the tail joint), and this mechanism is not attached to the ground, but we assume that it has the necessary support area for a stable motion over a frequencies' range. We want to focus the attention in two main aspects when the tail moves in an oscillating manner: The variation of the ZMP trajectory over the support area, and the force in the X direction (the advance direction in the biped case) that the tail produces at the joint axis and at the body mass m_b. First, we introduce the kinematics, dynamics y ZMP equations for this system, and then we will analyze them.

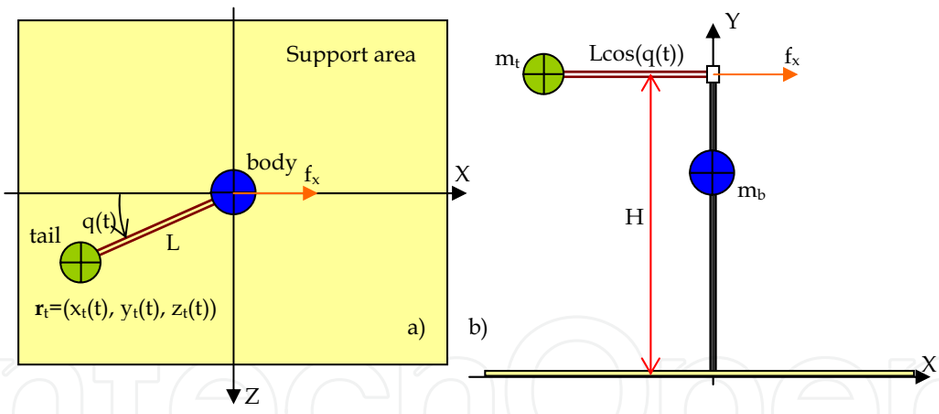

Figure 6. Horizontal pendulum: a) Top view, b) Sagittal view

The kinematic equations that relate the tail mass motion with the joint position are the following ones:

$$\begin{aligned} &x_t(t) = -L\cos(q(t)); && y_t(t) = H; && z_t(t) = L\sin(q(t)); \\ &\dot{x}_t(t) = L\sin(q(t))\dot{q}(t); && \dot{y}_t(t) = 0; && \dot{z}_t(t) = L\cos(q(t))\dot{q}(t); \\ &\ddot{x}_t(t) = L\sin(q(t))\ddot{q}(t) + L\cos(q(t))\dot{q}^2(t); && \ddot{y}_t(t) = 0; && \ddot{z}_t(t) = L\cos(q(t))\ddot{q}(t) - L\sin(q(t))\dot{q}^2(t); \end{aligned} \quad (22)$$

We obtain the dynamic equation by means of Newton-Euler Method. These equations provide the force **f**(t) that the tail exerts over the joint axis and body mass, and on the other hand, the needed joint torque τ(t) to produce a desired trajectory q(t).

$$\mathbf{f}(t)=\begin{bmatrix} f_x(t) \\ f_y(t) \\ f_z(t) \end{bmatrix} = -m_t \begin{bmatrix} \ddot{x}_t(t) \\ g \\ \ddot{z}_t(t) \end{bmatrix} = -m_t \begin{bmatrix} L\left[\sin(q(t))\ddot{q}(t)+\cos(q(t))\dot{q}^2(t)\right] \\ g \\ L\left[\cos(q(t))\ddot{q}(t)-\sin(q(t))\dot{q}^2(t)\right] \end{bmatrix} \tag{23}$$

$$\tau = I_{ty}\ddot{q}(t)+\mathbf{r}_t\times m_t\ddot{\mathbf{r}}_t = I_{ty}\ddot{q}(t)+m_t(z_t(t)\ddot{x}_t(t)-x_t(t)\ddot{z}_t(t)) = (I_{ty}+m_tL^2)\ddot{q}(t) \tag{24}$$

Parameters m_t and I_{ty} are the tail mass and Y-component of the inertial moment respectively. The total mass of this system is $M=m_t+m_b$, and the CoG is given by:

$$\mathbf{cog}=\frac{m_tL}{M}\left[-\cos(q(t)) \quad 0 \quad \sin(q(t))\right]^T \tag{25}$$

The general expression for the ZMP for an n-link system is (Vukobratovic et al., 1990):

$$zmp_x=\frac{\sum_{i=1}^{n} m_i\left(x_i\left(\ddot{y}_i+g\right)-y_i\ddot{x}_i\right)-I_{iz}\dot{\omega}_{iz}}{\sum_{i=1}^{n} m_i\left(\ddot{y}_i+g\right)}; \quad zmp_z=\frac{\sum_{i=1}^{n} m_i\left(z_i\left(\ddot{y}_i+g\right)-y_i\ddot{z}_i\right)-I_{ix}\dot{\omega}_{ix}}{\sum_{i=1}^{n} m_i\left(\ddot{y}_i+g\right)} \tag{26}$$

In the case of our simple pendulum, the ZMP vector is reduced to the expression 27, and we can see that it depends on three terms: a gravitational term, a centripetal term and an inertial term.

$$\mathbf{zmp}=\frac{m_t}{Mg}\begin{bmatrix} x_tg-y_t\ddot{x}_t \\ 0 \\ z_tg-y_t\ddot{z}_t \end{bmatrix} = \frac{m_tL_t}{Mg}\left((g+\dot{q}^2(t))\begin{bmatrix} -\cos(q(t)) \\ 0 \\ \sin(q(t)) \end{bmatrix} - H\ddot{q}(t)\begin{bmatrix} \sin(q(t)) \\ 0 \\ \cos(q(t)) \end{bmatrix} \right) \tag{27}$$

We analyze now these magnitudes when the mass m_t moves from one side of X axis to the other one. We consider that q(t) oscillates between the values of $-\pi/2$ and $\pi/2$, given this trajectory by a periodic function (a sinusoidal or triangular function, as an example). If this trajectory is symmetric, then at q(t)=0 radians, the joint velocity modulus will be maximum and the acceleration will be zero. At the trajectory limits $q(t)=\pm\pi/2$, when the joint changes its motion direction, the velocity will be zero, and the acceleration modulus will reach a maximum.

Using (23), we can see that when q(t) is within one of these limits, the force **f** is in the positive X direction, proportional to the acceleration, and tries to push the m_b mass in this positive direction. When the joint passes through the centre position q(t)=0, this force is in the negative X direction, proportional to the square of the joint velocity, and pushes the mass m_b in this negative direction. The magnitude of the f_x component thus varies in a periodic fashion with and oscillation frequency being twice the joint frequency.

Using now (25) and (27), the CoG always describes a circumference arc, while the ZMP will describe a trajectory depending on the joint trajectory selected. In the least case we can observe that the maximum and minimum values of the component zmp_x, which define the

minimum required length of the support area in this direction, are obtained by considering the velocity at the instant of q(t)=0 and the acceleration when the joint is in its extreme limits. These values are independent of the trajectory shape, while the maximum values in the zmp_z component will depend on the shape of the joint trajectory.

Since we mainly use sinusoidal trajectories in our biped system, we show in figure 7 the X component of the force **f** and the CoG and ZMP trajectories, for sinusoidal trajectories with frequencies 0.1, 0.2, 0.3, 0.4 and 0.5 Hz, given by (28), and considering masses and lengths values equal to 1 (m_t=m_b=L=H=1) in expressions (23), (25) and (27). We can observe how the component f_x, and also the maximum values of the ZMP components that define the necessary support area, grow in a way proportional to the square of the joint oscillation frequency ω.

$$q(t) = A\sin(\omega t); \quad \dot{q}(t) = A\omega\cos(\omega t); \quad \ddot{q}(t) = -A\omega^2\sin(\omega t); \tag{28}$$

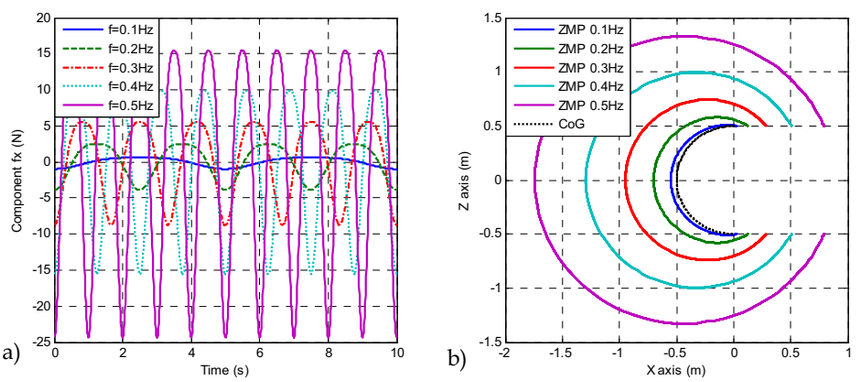

Figure 7. a) f_x component and b) ZMP and CoG for frequencies between 0,1Hz and 0,5Hz

5.2 Tail effect over an oscillating system

Now we consider a lower passive system that is able to oscillate in the X direction, just like our biped mechanism. In this case, the force exerted by the tail over the axis joint may be enough for producing the system oscillation, and in the biped case, the robot will be able to walk without the gravity effect shown in section 3, which we obtain using an equilibrium ankle position different from zero. In section 7 we will show the behaviour of the biped mechanism when the tail follows a sweep sinusoid (chirp function) (Berenguer & Monasterio, 2007) and the ankle joint equilibrium positions are zero. This study also allows to the observation of a designed system, its characteristics and behaviour over different frequencies: stability, periodicity, step length, consumption, etc.

The ZMP displacement will be affected by velocities and accelerations of the oscillating passive system, mainly in the X direction component, depending on the step length and collision magnitude at each frequency. The Z component will be almost the same as is estimated using (27) and allows to select the length of the support area and feet in the Z direction.

6. Power and energy consumption study

In this section we present solutions to reduce the power consumption of the system. On the one hand, we try to obtain a smooth contact between the feet and the ground in order to reduce the kinetic energy losses at the collisions. On the other hand, we will consider the design of a spring system at the tail joint to allow the robot to produce the tail oscillation with low power consumption. Let us remember that one of our main objectives is to obtain a periodic gait that can be maintained with minimum energy cost.

6.1 Smooth contact between the feet and the ground

In order to reach this objective we adjust the system parameters trying to reduce the foot velocity of the swing leg near zero at the contact instant. This velocity reduction involves less kinetic energy losses, and is obtained by means of reducing velocities of both ankle joints and the inclination velocity of the body at the same instant.

Ankle joint velocity will be zero if the joint is in a stable equilibrium state or if the joint oscillation is in a maximum position. The first situation is obtained easily for the swing leg by means of adjusting the friction coefficient B_{ank}. In the case of the stance leg, this first situation requires high friction, and we search the second option by adjusting the K_{ank} and θ_{0ank} spring parameters. In addition, this second option produces a longer step, compared to the first one, and less energy dissipation due to joint friction.

On the other hand, the inclination velocity of the body will be zero if the inclination angle α is reached at stable or a maximum position. That depends on the tail joint oscillation frequency and trajectory shape, and also on the top joint friction. Because we assumed this friction to be negligible, we try to adjust the trajectory amplitude so that the velocity is near zero when the angle reaches its maximum.

In the case of a real robot, it is important to mention that although the ankle parameters are mechanical parameters whose adjustment is not made by software, mechanisms like MACCEPA (Van Ham et al., 2006) allow for adjustment of the equilibrium position and the spring constant of this type of joints in real time. The parameter B_{ank} should be adjustable once for different gaits.

6.2 Adding a spring to the tail joint

The oscillatory motion of the tail requires high energy consumption if only one electric motor is used, since this motion involves successive accelerations and decelerations. In (Berenguer & Monasterio, 2006) we proposed adding a torsional spring to the tail joint that collaborates in performing this motion. The spring constant was selected by trial and error. In this work we propose to use the relation between torque and position of the tail without spring for selecting the stiffness using the slope of the line that fits this curve.

As an example, figure 8 shows the torque and position relation in the case of the last result presented in (Berenguer & Monasterio, 2007b), that will be our comparative experiment in the simulation results presented in section 7.

Figure 8.a presents both magnitudes versus time and we can see how the torque is quite different with respect to an unperturbed linear spring (sinusoidal torque). Figure 8.b shows torque versus joint position during eight strides and we can observe the nonlinearity of this relation and the phase shift between both signals (remember Lissajous curves). This figure also shows the line that fits the closed curve which expression is given by (29). The first

coefficient of this line equation is used as the stiffness parameter of the tail spring used in the simulation in next section.

$$\tau(t) = -0.03507 q_{tail}(t) + 3.931 \cdot 10^{-5} \quad (29)$$

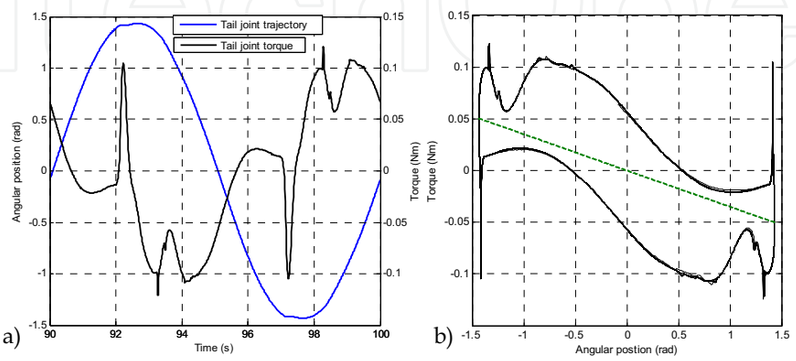

Figure 8. a) Joint position and torque vs. time, b) Joint torque vs. joint position and fitted line

7. Simulated models, tools and results

This section starts presenting the biped model parameters used in our simulations and the model of contact forces with the ground. Next we show the simulation environment and tools and finally the results of two experiments, one of them considers a low oscillation frequency of the tail, and the other one using a chirp function as the reference signal of the tail joint. The aim of this section is to show an example of the concepts and results in the previous sections.

7.1 Biped mechanism model parameters

The kinematic parameters and masses presented in table 1 are used in the simulations and in previous works (Berenguer & Monasterio, 2006 and 2007b). Their meaning is shown in figure 1. The simulated biped model is 460 mm tall, and its weight is 2050 gr.

Model Parameters					
Name	Value	Name	Value	Name	Value
M_{body}	50.0gr	L_{adv}	0.0mm	h_{top}	30.0mm
M_{top}	50.0gr	L_{bar}	400.0mm	h_{bar}	200.0mm
M_{bar}	200.0gr	L_{foot}	10.0mm	h_{foot}	5.0mm
M_{foot}	200.0gr	L_{tail}	150.0mm	h_{tail}	20.0mm
M_{leg}	650.0gr	d	50.0mm	----	----
M_{tail}	700.0gr	M_T	2050.0gr	H_T	460.0mm

Table 1. Biped model parameters used in simulations

7.2 Estimation of the Ground Reaction Force and ZMP

We consider as contact points $\mathbf{p}_i$ between the biped and the ground, the four corners of the area of each foot, and for each contact point, the ground reaction force ($\mathbf{f}_i$) is simulated using (30). Fig. 9 shows the XYZ directions and an example of vectors $\mathbf{f}_i$, $\mathbf{p}_i$ and the velocity $\mathbf{v}_i$ of $\mathbf{p}_i$. We assume that the ground is flat with no slope at the height y=0.

$$\mathbf{f}_i = \begin{cases} (0 \quad 0 \quad 0)^T & p_{yi} \geq 0 \\ -(1000\, v_{ix} \quad 10000\, p_{iy} + 2000\, v_{iy} \quad 1000\, v_{iz})^T & p_{yi} < 0, v_{iy} < 0 \\ -(1000\, v_{ix} \quad 10000\, p_{iy} \quad 1000\, v_{iz})^T & p_{yi} < 0, v_{iy} \geq 0 \end{cases} \tag{30}$$

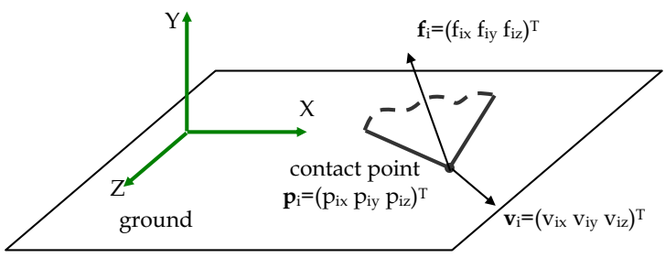

Figure 9. Ground reaction force at a foot contact point $\mathbf{p}_i$

In this model, when the contact point goes into the ground, there is friction in the Y direction. When it tries to take-off, there is no friction in this direction.

The sum of the vertical components f_{iy} of the eight contact points, equation (31), defines the vertical component F_{TY} of the total ground reaction force $\mathbf{F}_T$, and its average distribution of the position on XZ plane, equation (32), defines the position of the ZMP.

$$F_{TY} = \sum_{i=1}^{8} f_{iy} \tag{31}$$

$$zmp_x = \frac{\sum_{i=1}^{8} p_{ix} f_{iy}}{F_{TY}}; \quad zmp_z = \frac{\sum_{i=1}^{8} p_{iz} f_{iy}}{F_{TY}} \tag{32}$$

7.3 Simulation environment

The system has been programmed using Matlab and SimMechanics Toolbox of Simulink. The main system and subsystems are the following:

- *Main system*: This system represents the complete model and environment (ground contact) and is shown in Figure 10. Functional Simulink blocks represent links, joints, springs with friction and the ground and tail subsystems. Sensor and scope blocks are used for data record.

- *Tail subsystem*: Shown in figure 11, it contains besides the joint and link blocks, the tail reference trajectory, the joint control and the tail spring blocks. Blocks on the right side are used to estimate the mechanical power (product of joint torque and angular velocity of the tail) and the integral of its absolute value, represents the (mechanical) energy provided by the actuator and the total energy consumption of the overall system.
- *Ground model contact subsystem*: This subsystem (Figure 12) simulates the ground by means of equation (30) at each contact point and estimates the normal ground reaction force F_{TY} and the ZMP coordinates using (31) and (32). This subsystem also provides the position of each foot corner in the Y direction, which allows us to observe when the foot leaves the ground and also the foot elevation during walking.

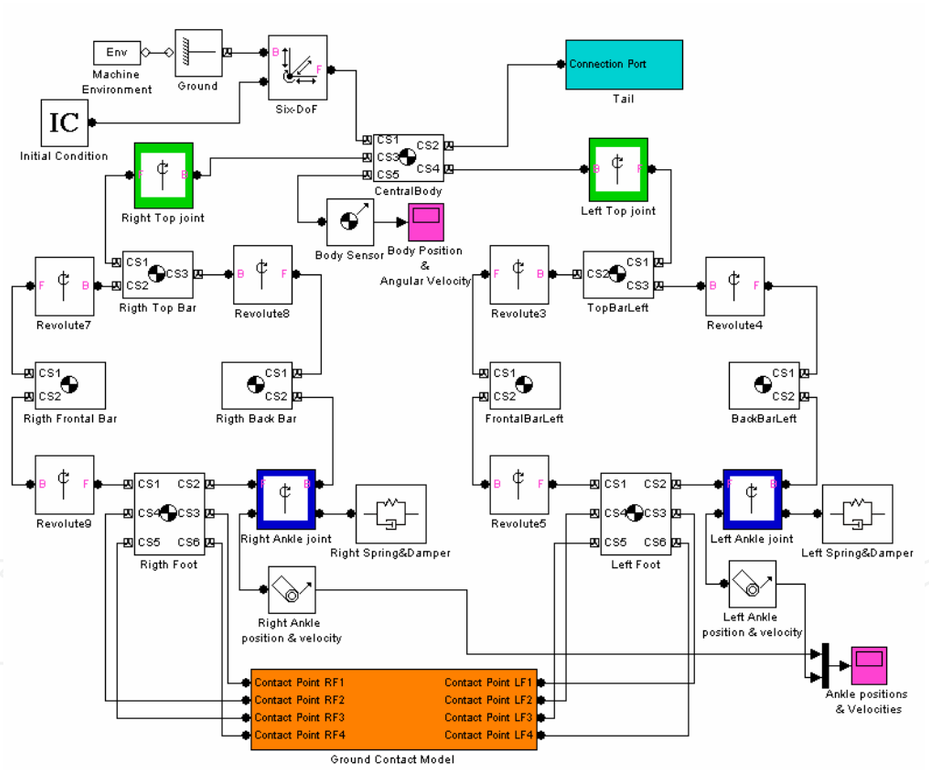

Figure 10. Main Simulink system that represent the simulated biped model and its environment

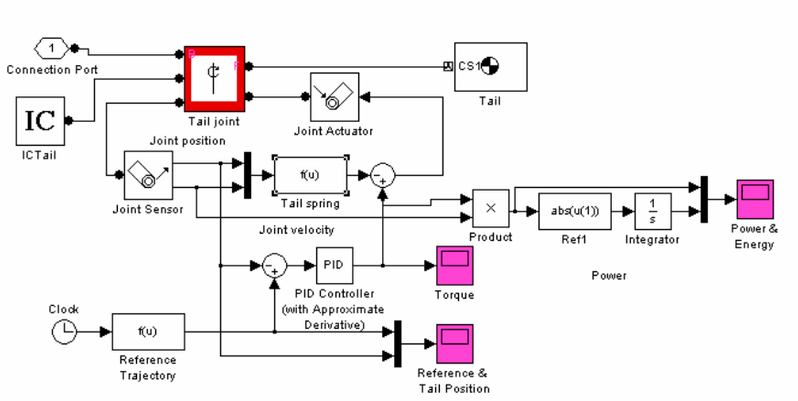

Figure 11. Blocks and signals into the Tail subsystem

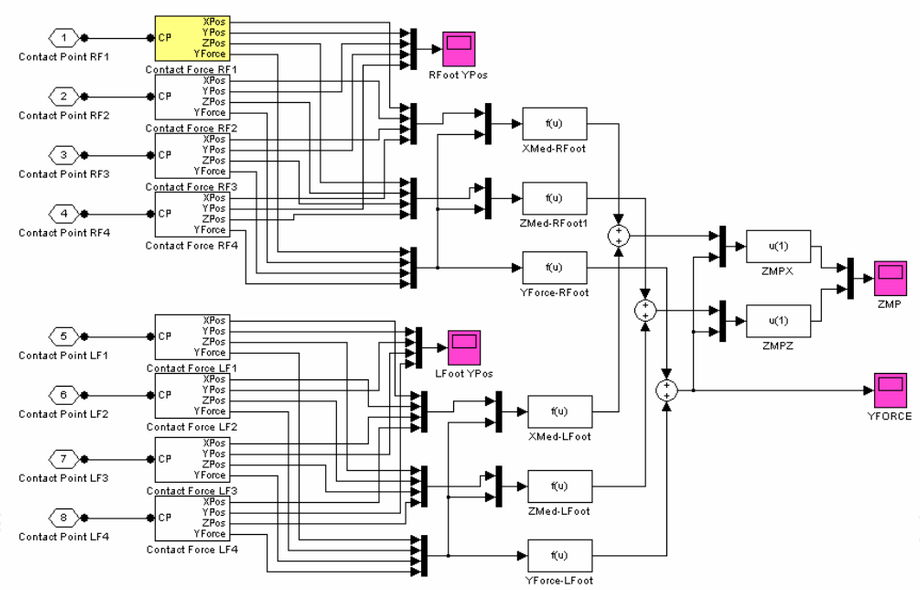

Figure 12. Ground contact model subsystem

7.4 Simulation results at low frequency

This section presents simulation results using a sinusoidal reference trajectory for the tail joint at 0.1Hz constant frequency given by expression (33), and adding a torsional spring to this joint with the constant K_{tail}=0.03507 from (29). The amplitude of the reference signal and the ankle joint springs parameters have been adjusted in order to reduce the normal reaction

force of the ground at contact instant. The values of these parameters are presented in Table 2.

$$q_{ref}(t)=\begin{cases}\dfrac{A_{tail}}{2}(1-\cos(2\omega_s t)) & 0s \le t < 2.5s \\ A_{tail}\cos(\omega_s(t-2.5)) & 2.5s \le t < 102.5s \\ \dfrac{A_{tail}}{2}(1+\cos(2\omega_s(t-102.5))) & 102.5s \le t < 105s \\ 0 & 105s \le t\end{cases} \quad (33)$$

ω_s (rad/s)	A_{tail} (rad)	K_{tail} (Nm/rad)	K_{ank} (Nm/rad)	B_{ank} (Nms/rad)	θ_{0ank} (rad)	Foot size (mm^2)
0.2π	1.49	0.03507	8.4	0.4	-0.038	200x85

Table 2. Parameters in the first experiment at 0,1Hz stride frequency

The aim of these results is to give an overview of the general behaviour of the mechanism, and on the other hand, to compare the consumption results with our previous results presented in (Berenguer & Monasterio, 2007b), using the same model without the torsional spring at the tail joint.

We start analyzing the tail behaviour. Figure 13.a shows the reference signal given by (33), the trajectory of the tail $q_{tail}(t)$, and the tracking error. We use a PD control with gains K_P=1 and K_D=0.5 instead of a proportional control, because it provides smoothness to all joints motions, including the passive joints (Berenguer & Monasterio, 2007b). Figure 13.b shows the joint torque versus $q_{tail}(t)$, and if we compare it with figure 8.b, we can observe the effect of the tail spring in the exerted joint torque.

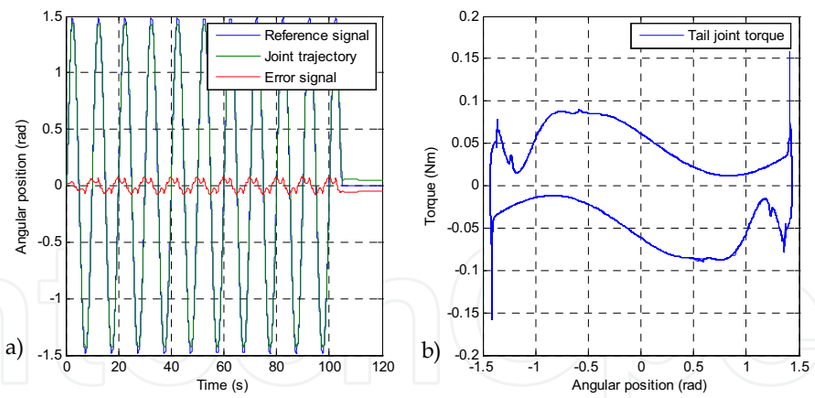

Figure 13. a) Constant frequency reference trajectory for the tail joint, performed trajectory and error signal; b) Joint toque vs. joint position

Next we present the ankle's joint behaviour. Figures 14.a and 14.b show the ankle positions and velocities of both legs during a stride. In the second one the double support phase corresponds to the overlapping of both velocities, while in the single support phase the leg velocities are different.

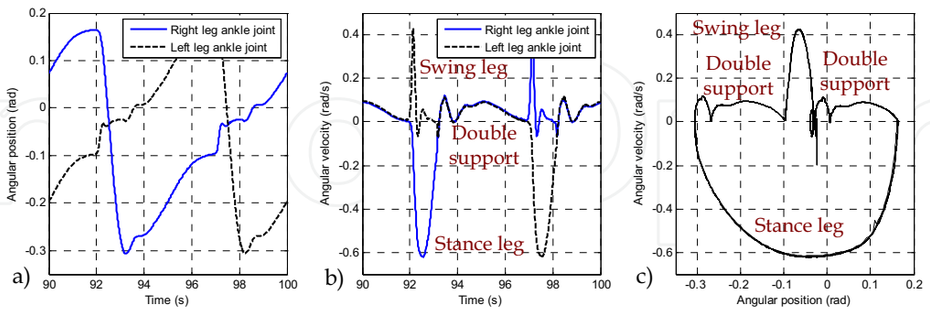

Figure 14. a) Ankle joint positions and b) velocities; c) Right leg phase diagram

The velocity of the swing leg easily reaches the zero value, and the velocity of the stance leg has a value near -0.2rad/s at the contact instant. Figure 14.c shows the phase diagram of the right leg during the eight strides between instants t=20s and t=100s, so we can evaluate the periodicity of the gait. We can also identify in this figure the double support phases (they have the same shape), and when the leg is the stance leg and the swing leg.

Now we analyze the body inclination velocity and the contact with the ground. Figure 15 shows this velocity and the normal component of the ground reaction force F_{TY}. This last magnitude is a measure of the smoothness of the contact and we can see its variation with respect to the value due to the weight of the robot (near 20N) at the collision instant.

Figure 16.a shows the ZMP displacement during one stride between instants t=90s and t=100s. This ZMP trajectory is similar to the CoG trajectory presented in section 4.3 (Figure 5), but we can also notice here the effect of the collision that generates a peak in the forward X direction. The short length of this collision effect is better observed in figure 16.b.

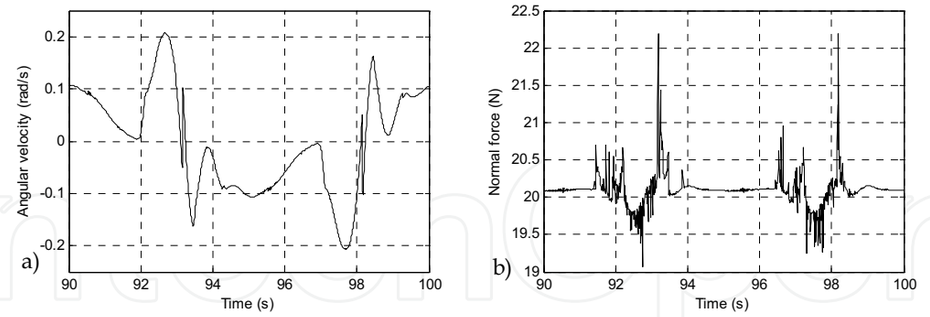

Figure 15. a) Inclination angle velocity and b) normal component of the ground reaction force

Finally, figure 17 shows the body position in the X direction and the mechanical energy consumed by the tail joint. This figure presents the results of the simulations together with the last results in (Berenguer & Monasterio, 2007b). In that work, without a tail spring, the only different parameters were A_{tail}=1.443rad and θ_{0ank}=0.036rad. The main result from the

comparison of both experiments is that using a tail spring we can reduce the consumption without reducing the crossed distance. In the presented example, the energy consumption reduces in 10.68% and the crossed distance increases in 3.4%.

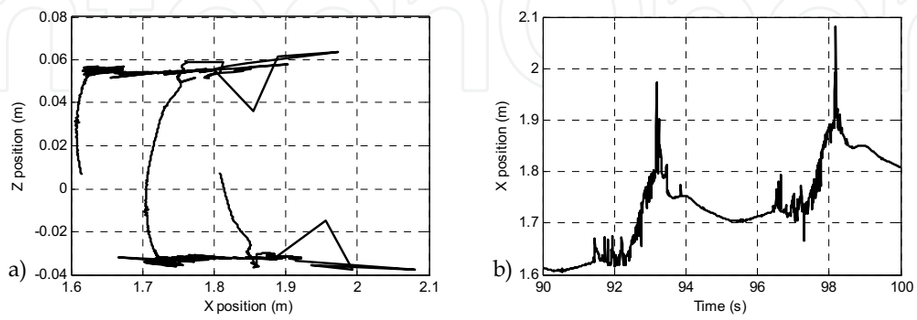

Figure 16. a) ZMP displacement and b) X component of the ZMP during one stride

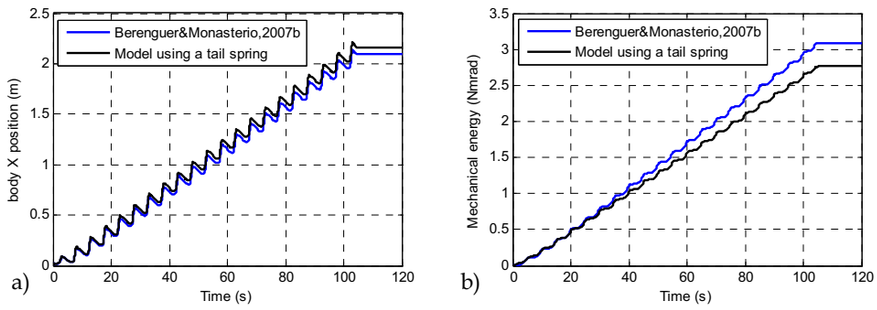

Figure 17. a) Body position and b) mechanical energy consumption

7.5 System behaviour variation with frequency

Now we present simulation results when the frequency of the tail trajectory varies its oscillation frequency. We use the biped model again without the tail spring (K_{tail}=0), and in this simulation the equilibrium ankle positions are zero (θ_{0ank}=0), and therefore, if the biped walks, it is due to the force exerted in the forward direction by the tail motion. The tail trajectory is given by (34) and has amplitude $\pi/2$. Also the feet area was enlarged to 300x185mm^2 to ensure a stable gait at all frequencies. The tail trajectory is shown in Figure 18.a, and its oscillation frequency varies from 0 to 0,5Hz in 150 seconds. The distance walked and mechanical energy consumption are shown in figure 18.b.

$$q_{ref}(t) = \frac{\pi}{2}\sin(0.0105t^2) \tag{34}$$

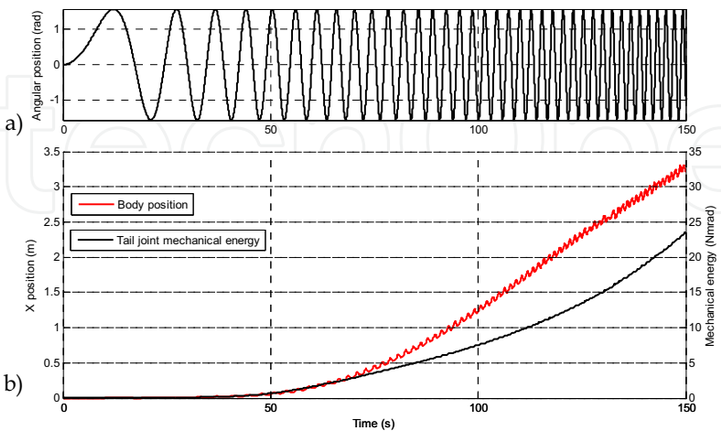

Figure 18. a) Tail joint reference trajectory and, b) body position and energy consumption

The biped performs its first step at t=20s, when the instantaneous frequency is 0.067Hz, and the longest steps (L_{step}=60mm) are obtained between times t=94s and t=114s, corresponding to frequencies 0.31Hz and 0.38Hz. We also notice that after t=125s (0.42Hz), the gait losses its periodic behaviour partially.

Finally, figure 19 shows both ZMP components versus time. We can see the effect of collisions with the feet and the ground, and in the Z component case, how its amplitude grows with frequency.

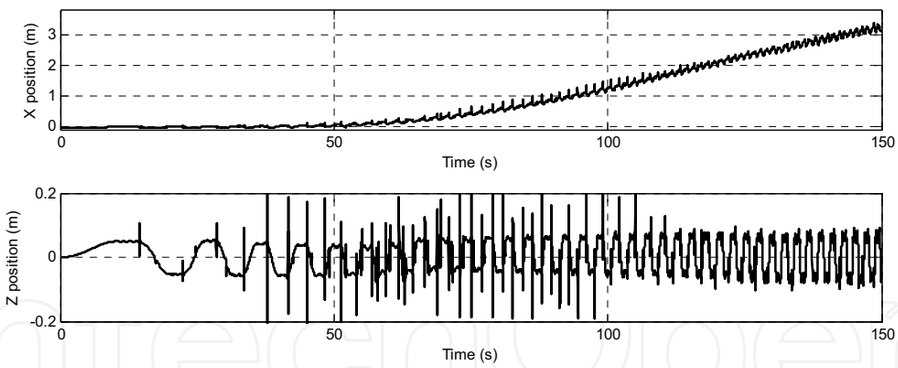

Figure 19. ZMP trajectory: zmp_x and zmp_z components versus time

8. Real prototype robot Zappa

We built the biped prototype Zappa following our kinematic model. The first version was presented in (Berenguer & Monasterio, 2006), and now we present a new version based on the results in this work. Figure 20 shows both versions of Zappa. The main mechanical modifications are the following ones: the tail location is now below the top joints, the top joints are made up using hinges and the feet have been enlarged in the forward direction.

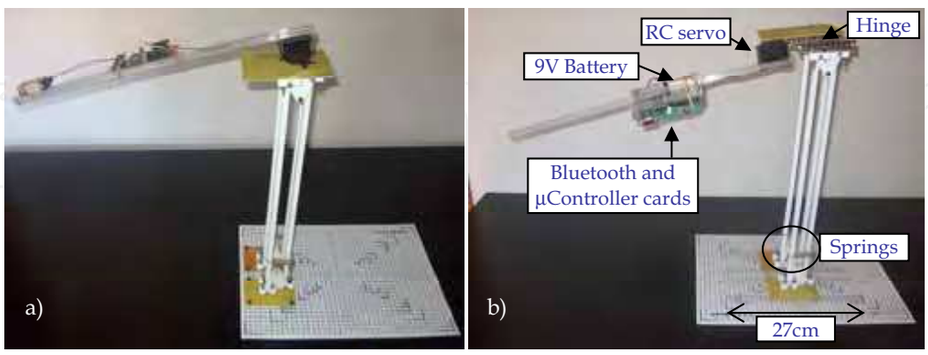

Figure 20. a) First and b) second versions of the robot prototype Zappa

The electronic components are a commercial microcontroller card with a PIC16F877A, a communication Bluetooth module eb500 and a commercial RC servo (max. 180º rotation). The prototype is powered by a 9V battery (170mAh approx. – 6LR type) that supplies all electrical power and all the electronics components are distributed in the tail, as shown in Figure 20. Figure 21 shows Zappa robot performing a stride in 4.56 seconds. Time instants are indicated in each photo.

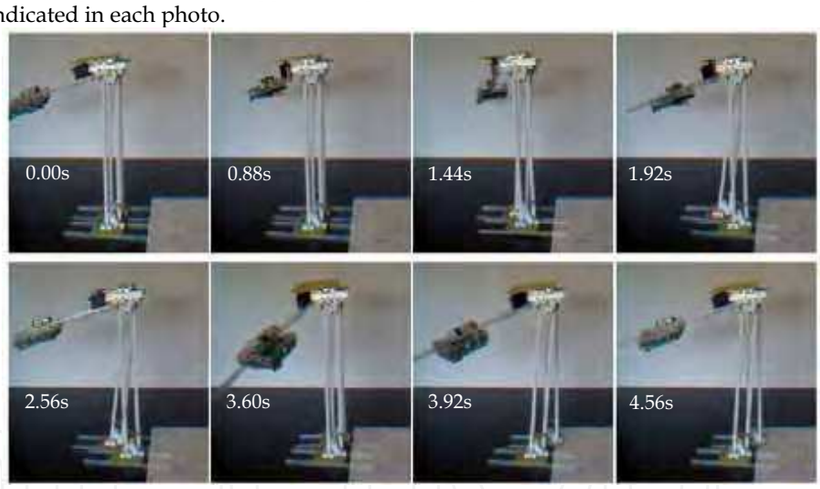

Figure 21. Biped prototype Zappa performing two steps

9. Summary, conclusions and future work

We have presented in this work a biped mechanism of easy design and construction that is able to walk with only one actuator. The system is attractive for educational and commercial applications due to the simplicity of the applied concepts. In order to reduce the energy consumption of this system, an important problem in actuated bipedal locomotion, we aim for a gait with smooth contact between feet and ground, reduce the joints friction and

include an additional torsional spring to reduce the needed torques at the actuated tail joint. This system walks thanks to a combination of the gravitational force and the force exerted by the tail joint over the body and legs. The resulting biped represents a system half way between traditional actuated biped robots and dynamic passive robots. We have also built a low cost biped prototype that validates our model and shows the simplicity and the minimum number of required components.

Future work will be focused on improving the model, by means of adding new joints at the feet and knees; improving the prototype, by means of equipping Zappa with sensors (Force sensors, encoders, accelerometer and compass for example); and the design and implementation of an adaptive scheme that will allow the robot to adjust its parameters in real time and search for optimal gaits. We will consider also new situations such as walking down a slope, on one hand, which will allow us to compare this model with pure passive biped mechanisms, and on the other hand, the existence of obstacles and holes that impose non periodic gait and dynamical variation of the step length.

10. References

Alexander, R.M. (2005). Walking made simple. *Science Magazine*, Vol. 308, pp. 58-59, 2005.

Ambrose, R.; Zheng, Y. & Wilcox, B. (2006). Humanoids, *International Assessment of Research and Development in Robotics*, World Technology Evaluation Center, Inc, pp. 41-54, 2006.

Berenguer, F. J. & Monasterio-Huelin, F. (2006). Easy design and construction of a biped walking mechanism with low power consumption, *Proceedings of the 9th Int. Conf. on Climbing and Walking Robots*, pp. 96-103, Brussels, September 2006.

Berenguer, F. J. & Monasterio-Huelin, F. (2007). Trajectory planning using oscillatory chirp functions applied to bipedal locomotion, *Proceedings of the 4th Int. Conf. on Informatics in Control, Automation and Robotics*, Vol. RA-2, pp. 70-75, Angers, May 2007.

Berenguer, F. J. & Monasterio-Huelin, F. (2007b). Stability and smoothness improvements for an underactuated biped with a tail, *Proceedings of the 2007 IEEE Int. Symp. on Industrial Electronics*, pp. 2083-2088 , Vigo, June 2007.

Collins, S.; Ruina, A.; Tedrake, R. & Wisse, M. (2005). Efficient bipedal robots based on passive dynamic walkers, *Science Magazine*, Vol. 307, pp. 1082-1085, 2005.

Gomes, M. & Ruina, A. (2005). A walking model with no energy cost, In revision, *Phys Rev E*, 2005.

Kuo, A. D. (1999). Stabilization of lateral motion in passive dynamic walking, *The International Journal of Robotics Research*, Vol.18, No.9, pp. 917-930, 1999.

Iida, F. & Pfeifer, R. (2006). Sensing through body dynamics, *Robotics and Autonomous Systems*, Vol.54, pp. 631–640, 2006.

Kajita, S.; Nagasaki, T.; Kaneko, K. & Hirukawa H. (2007). ZMP-Based Biped Running Control, The HRP-2LR Humanoid Biped Robot, *IEEE Robotics & Automation Magazine*, pp. 2-12, June, 2007.

McGeer, T. (1990). Passive dynamic walking, *The International Journal of Robotics Research*, Vol. 9, No. 2, pp. 62-82, 1990.

Pfeifer, R. & Scheier, C. (1999). Understanding Intelligence, *MIT Press*, Cambridge, MA, 1999.

Takita, K.; Katayama, T. & Hirose, S. (2003). Development of Dinosaur-like Robot TITRUS - The Efficacy of the Neck and Tail of Miniature Dinosaur-like Robot TITRUS III, *Proceedings of the 2003 IEEE Int. Conf. on Robotics & Automation*, pp. 2466-2471, Taipei, Taiwan, September, 2003.

Van Ham, R.; Van Damme, M.; Vanderborght, B.; Verrelst, B. & Lefeber, D. (2006). MACCEPA: The mechanically adjustable compliance and controllable equilibrium position actuator, *Proceedings of the 9th Int. Conf. on Climbing and Walking Robots*, Brussels, pp. 196-203, September 2006.

Vukobratovic, M. & Juricie, D. (1969). Contribution to the synthesis of biped gait, *IEEE Transactions on Bio-Medical Engineering*, Vol.16, No.1, pp. 1-6, 1969.

Vukobratovic, M.; Borovac, B.; Surla, D. & Stokic, D. (1990). Biped locomotion: Dynamics, stability, control and application, *Springer-Verlag*, 1990.

Wahde, M. & Pettersson, J. (2002). A brief review of bipedal robotics research, *Proceedings of the 8th UK Mechatronics Forum International Conference (Mechatronics 2002)*, pp. 480-488, 2002.

Bioinspiration and Robotics Walking and Climbing Robots

Edited by Maki K. Habib

ISBN 978-3-902613-15-8
Hard cover, 544 pages
Publisher I-Tech Education and Publishing
Published online 01, September, 2007
Published in print edition September, 2007

Nature has always been a source of inspiration and ideas for the robotics community. New solutions and technologies are required and hence this book is coming out to address and deal with the main challenges facing walking and climbing robots, and contributes with innovative solutions, designs, technologies and techniques. This book reports on the state of the art research and development findings and results. The content of the book has been structured into 5 technical research sections with total of 30 chapters written by well recognized researchers worldwide.

InTech Europe
University Campus STeP Ri
Slavka Krautzeka 83/A
51000 Rijeka, Croatia
Phone: +385 (51) 770 447
Fax: +385 (51) 686 166
www.intechopen.com

InTech China
Unit 405, Office Block, Hotel Equatorial Shanghai
No.65, Yan An Road (West), Shanghai, 200040, China
中国上海市延安西路65号上海国际贵都大饭店办公楼405单元
Phone: +86-21-62489820
Fax: +86-21-62489821

IntechOpen